Geophysical Research Letters

RESEARCH LETTER
10.1029/2022GL100815

Key Points:

- We estimate Bennu's phyllosilicate content is primarily Mg-rich serpentine with smaller amounts of cronstedtite and saponite
- We predict higher cronstedtite and lower Mg-rich serpentine abundances in the equatorial region and vice versa for the middle latitudes
- We observe thermal emission spectrometer spectral variability between the equatorial and middle latitude regions of Bennu that may be due to sorting effects

Supporting Information:

Supporting Information may be found in the online version of this article.

Correspondence to:

L. B. Breitenfeld,
laura.breitenfeld@stonybrook.edu

Citation:

Breitenfeld, L. B., Rogers, A. D., Glotch, T. D., Kaplan, H. H., Hamilton, V. E., & Christensen, P. R. (2022). Mapping phyllosilicates on the asteroid Bennu using thermal emission spectra and machine learning model applications. *Geophysical Research Letters*, *49*, e2022GL100815. https://doi.org/10.1029/2022GL100815

Received 12 AUG 2022
Accepted 7 OCT 2022

Author Contributions:

Conceptualization: L. B. Breitenfeld, A. D. Rogers, T. D. Glotch, P. R. Christensen
Formal analysis: L. B. Breitenfeld
Funding acquisition: A. D. Rogers, T. D. Glotch
Investigation: L. B. Breitenfeld, H. H. Kaplan
Methodology: L. B. Breitenfeld, A. D. Rogers, T. D. Glotch, V. E. Hamilton, P. R. Christensen
Project Administration: A. D. Rogers, T. D. Glotch
Software: L. B. Breitenfeld, A. D. Rogers
Supervision: A. D. Rogers, T. D. Glotch
Validation: L. B. Breitenfeld
Visualization: L. B. Breitenfeld, H. H. Kaplan

Mapping Phyllosilicates on the Asteroid Bennu Using Thermal Emission Spectra and Machine Learning Model Applications

L. B. Breitenfeld[1], A. D. Rogers[1], T. D. Glotch[1], H. H. Kaplan[2], V. E. Hamilton[3], and P. R. Christensen[4]

[1]Department of Geosciences, Stony Brook University, Stony Brook, NY, USA, [2]NASA Goddard Space Flight Center, Greenbelt, MD, USA, [3]Department of Space Science, Southwest Research Institute, Boulder, CO, USA, [4]School of Earth and Space Exploration, Arizona State University, Tempe, AZ, USA

Abstract Bennu, the target of the OSIRIS-REx mission, is an asteroid with compositions analogous to low petrologic type CI, CM, CR, and/or ungrouped carbonaceous chondrites. Asteroids like Bennu provide information about the building blocks of the early Solar System. Analysis of the mid-infrared remote sensing data informs mineral quantification. We apply a phyllosilicate specific model, developed by Breitenfeld et al. (2021, https://doi.org/10.1029/2021je007035) that distinguishes between Mg and Fe serpentines, to Baseball Diamond 1 (BBD1), equatorial station 3 (EQ3), and touch-and-go OSIRIS-REx thermal emission spectrometer data. The average total phyllosilicate predictions are 73 (BBD1) and 72 vol% (EQ3). We observe higher Fe-cronstedtite and lower Mg-rich serpentine content in the equatorial region of Bennu than average. Mid-infrared spectral variability may be explained by sorting effects through mass movement.

Plain Language Summary Bennu is an asteroid made of primitive materials that provide information about the early Solar System. Using infrared emission spectra and machine learning modeling, we estimate the amount and composition of phyllosilicate minerals across the surface of Bennu. Our results suggest that Bennu is primarily composed of phyllosilicate minerals as expected from previous studies. Mg- and Fe-rich serpentine abundances are mapped across the asteroid Bennu. Near the equator, our model predicts higher cronstedtite (Fe-rich serpentine) and lower Mg-rich serpentine compared to the average composition of the asteroid. The spectral and compositional variability on Bennu can be explained by aqueous processing and sorting effects.

1. Introduction and Background

Bennu is a near-Earth asteroid with a composition corresponding to low petrologic type (and sub-type) CI, CM, CR, and/or ungrouped carbonaceous chondrites (Hamilton et al., 2019, 2021, 2022; Lauretta et al., 2019). These primitive chondritic meteorites record early Solar System processes such as aqueous alteration. Given the primitive nature of Bennu, the target of the sample return mission OSIRIS-REx (Origins, Spectral Interpretation, Resource Identification, and Security–Regolith Explorer), it is important to analyze the remote sensing data such as the thermal emission spectrometer (OTES) data (Christensen et al., 2018) for mineralogical characterization. Understanding the composition of Bennu spatially informs large-scale asteroid mechanisms such as mass movement and sorting. Additionally, examining Bennu at local scales using individual OTES spectra is important for understanding specific locations such as the sampling site Nightingale.

Magnetite (555, 340 cm^{-1}) and phyllosilicate (e.g., 440 cm^{-1}) spectral features are apparent in OTES spectra of Bennu as well as a broad bowl-shaped feature (~1,100–650 cm^{-1}) corresponding to the silicate stretching region (Hamilton et al., 2019, 2021). The emissivity maximum around 528 cm^{-1} is consistent with high phyllosilicate (>78 vol%) and low olivine (<10 vol%) content (Hamilton et al., 2021). Carbonates (Kaplan et al., 2020) and rare exogenous pyroxene (DellaGiustina et al., 2021) were detected by other OSIRIS-REx instruments but are not spectrally dominant in the OTES datasets.

Hamilton et al. (2021) isolated two OTES type spectra (T1 and T2). T1 is interpreted as primarily coarsely particulate to rocky materials while T2 likely includes a thin coating or mixture of fine particulates (Hamilton et al., 2021). Hamilton et al. (2021) concluded that there is no evidence for major compositional variation on Bennu. Breitenfeld et al. (2021) used machine learning models to predict mineral volumetric abundances for Bennu's T1, T2, and OTES global average. The average spectrum was estimated as 78% phyllosilicate, 9% olivine,

Writing – original draft: L. B. Breitenfeld
Writing – review & editing: L. B. Breitenfeld, A. D. Rogers, T. D. Glotch, V. E. Hamilton

11% carbonates, 6% magnetite, and no pyroxene. T1 and T2 predictions were similar to the global average with variations ≤6 vol% depending on the mineral species.

Here we expand on previous studies, to understand OTES spectral variability. We use a partial least squares (PLS) machine learning model from Breitenfeld et al. (2021). We focus our attention on the Baseball Diamond 1 (BBD1) and equatorial station 3 (EQ3) datasets because of their high signal-to-noise ratio (SNR) compared to other OTES datasets. We present quantitative phyllosilicate mineralogy maps of the asteroid Bennu and consider potential causes for spectral heterogeneity across the surface. Finally, we analyze the phyllosilicate predictions at Nightingale and predict the phyllosilicate abundance of the sample that will be delivered to Earth in September 2023.

2. Methods

This study builds on previous work (Breitenfeld et al., 2021) focused on the development of mid-infrared models for the prediction of modal mineralogy of the asteroid Bennu. The phyllosilicate model from this study relies on a training set of mineral mixture samples. These samples have a wide compositional range and incorporate fine (<50 μm), coarse (>125 μm or pellet), and mixtures of these particle sizes. The collection of the laboratory spectral training set and the establishment of PLS coefficients are detailed in Breitenfeld et al. (2021).

Instead of applying models to average OTES spectra, as in Breitenfeld et al. (2021), here we apply the model to individual OTES spectra. This change requires the reduction of PLS coefficients from 1,500 to 310 cm^{-1} to 1,200–310 cm^{-1} because of wavelength-dependent noise in individual OTES spectra. We also changed the normalization method of the laboratory data set to match the OTES calibration pipeline methodology (Christensen et al., 2018, 2019a).

Within the model specifically tailored to phyllosilicates, three phyllosilicate mineral end-members are included (Mg-rich serpentine, cronstedtite, and saponite) making the prediction of each possible. For this investigation, we apply the phyllosilicate model to the BBD1 and EQ3 datasets. We select spectra with emission angles <55°, maximum brightness temperatures (MBT) >304 K, quality flags ranging from 0 to 2, and fully on-body measurements. OTES calibration, metadata, spectral measurements, and quality markers are detailed in the Planetary Data System (Christensen et al., 2019b) and by Hamilton et al. (2019, 2021). Based on these constraints, the BBD1 and the EQ3 datasets consist of 4,703 and 2,413 spectra with local true solar time (LTST) ranging from 8:54 a.m. to 4:12 p.m. and 12:12 p.m. to 12:36 p.m. The heliocentric distance differs for the two datasets with measurements occurring at ∼1 AU (BBD1) and ∼1.2 AU (EQ3) (Rozitis et al., 2020). These factors result in higher MBT for BBD1 (∼329–376 K) compared to EQ3 (∼304–337 K).

Unlike other spectral modeling techniques, PLS cannot produce modeled spectra to directly compare to OTES spectra. Therefore, we use spectral angle mapper (SAM) (Kruse et al., 1993) to check whether the prediction values are linked to spectral shape. First, we isolate OTES spectra with low and high prediction values for Mg-rich serpentine, cronstedtite, and saponite to create 1st and 99th percentile averages of each mineral species. Next, we compare the individual spectra of the OTES datasets to the 1st and 99th percentile averages for each mineral using SAM. When the model results correspond with spectral shape, low SAM scores (best matches) are associated with low prediction values for the 1st percentile average and high prediction values for the 99th percentile average.

For mineral species where we observe that spectral variability is linked to the prediction results, we create mineral maps of Bennu. The maps rely on the output of mineral prediction values in vol% from the phyllosilicate model applied to individual OTES spectra. Finally, we compile the maps using the MatLab program "makeMaps.m" (Ferrone et al., 2019) by averaging the prediction values of all the spots that fall within a given facet of the shape model of Bennu.

3. Results

The cross-validated root-mean-square error of the phyllosilicate model used in this study is 15.0 vol%. The average volumetric abundances for the BBD1 data set are 49% Mg-rich serpentine, 15% cronstedtite, and 8% saponite. The EQ3 data set average abundances are comparable at 52% Mg-rich serpentine, 14% cronstedtite, and 7% saponite (Figure 1). In Figure 2 (left), we compare the 1st and 99th percentile averages of the Mg-rich

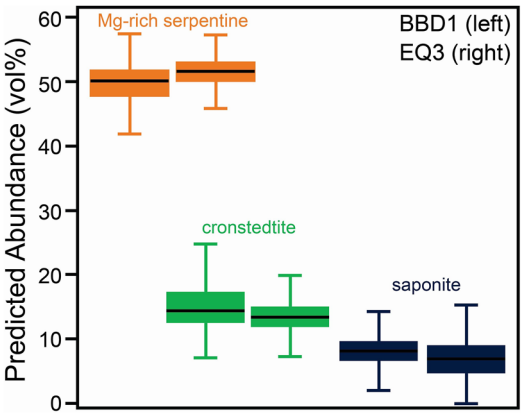

Figure 1. Box-and-whisker plot of Mg-rich serpentine, cronstedtite, and saponite prediction abundances for the baseball diamond 1 (BBD1) (left) and equatorial station 3 (EQ3) (right) datasets. Black lines represent median values, boxes indicate first and third quartile, and whiskers denote data range. Outliers (1.5 times the interquartile range smaller/larger than the first/third quartile) are omitted.

serpentine predictions for both the BBD1 (<~39.8 and >~55.0 vol% consisting of 47 spectra each) and EQ3 (<~44.2 and >~56.6 vol% consisting of 24 spectra each) datasets. We also include laboratory reference spectra from Breitenfeld et al. (2021) of coarse and fine particulate Mg-rich serpentine with the OTES pipeline calibration applied. We observe similar spectral shapes for the percentile averages between the two datasets. The standard deviation for each of the OTES channels is smaller for BBD1 compared to EQ3. In contrast to the 1st percentile average spectrum, the 99th percentile average spectrum's Christiansen feature (CF) shifts to a higher wavenumber position (~8.66 cm^{-1} shift), the silicate stretching feature is deeper, and the spectrum has a positive slope between ~650 and ~530 cm^{-1}.

Figure 2 (right) shows the 1st and 99th percentile average spectra of cronstedtite for the BBD1 (<~9.0 and >~26.6 vol%) and EQ3 (<~8.5 and >~20.5 vol%) datasets. Like the Mg-serpentine spectra, we observe similar spectral shapes for the percentile averages between the datasets. Compared to the 1st percentile average, the 99th percentile average (particularly for the BBD1 data set) has higher emissivity values in the silicate stretching region and lower emissivity values for the 440 cm^{-1} feature.

We did not observe spectral variability between the 1st and 99th percentile averages of saponite. For this reason, we did not map saponite abundances across the surface of Bennu. Potential reasons for the lack of spectral variability associated with the saponite variable are: (a) the model did not isolate saponite's spectral variability, (b) the saponite abundance is too low to cause spectral variability (Figure 1), or (c) the saponite content is relatively homogeneous across Bennu. Any or all of these factors may influence the lack of spectral variability between the spectra with low and high saponite predictions.

To determine if there is an association between spectral shape and mineral predictions, we investigate OTES SAM scores (Figure S1 in Supporting Information S1). Note, we do not anticipate a perfect one-to-one relationship between SAM score and prediction abundances since two spots can theoretically have the same abundance of the material in question while having different proportions of the remaining constituents resulting in two different spectral shapes. For the BBD1 data set, low SAM scores (best matches) are associated with low prediction values for the 1st percentile average and high prediction values for the 99th percentile average. In the case of Mg-rich serpentine and cronstedtite, this association is present for the BBD1 data set and weakly holds for the EQ3 data set. A wider prediction abundance range exists for both Mg-rich serpentine and cronstedtite for the BBD1 data set compared to the EQ3 data set. This, along with the weaker correlation between EQ3 SAM scores and abundances, is likely due to differences in spectral contrast and SNR between the two datasets as discussed below.

The OTES datasets possess differences in sampling conditions that affect spectral measurements. Factors such as orbital distance and LTST influence MBT which in turn affect SNR, spectral contrast, and material contributions (coarse vs. fine particulates). We anticipate that the BBD1 data set predictions are more accurate compared to the EQ3 data set due to the higher SNR. There is no clear correlation between the prediction abundances of individual OTES spots and their MBT or LTST (Figure S2 in Supporting Information S1). If particle size was entirely responsible for the observed spectral variability, we would expect a correlation because at different temperatures the ratio of coarse to fine particulate contributions change in the mid-infrared. This indicates that particle size is not solely contributing to observed spectral differences.

From the machine learning predictions, we constructed mineral maps. We chose to prioritize the BBD1 maps because we observed greater spectral variability and a clearer link between spectral shape and the prediction abundances in the BBD1 data set. This can be explained by the higher MBT of BBD1 compared to EQ3 (Figure S2 in Supporting Information S1) improving the SNR. The maps for Mg-rich serpentine and cronstedtite are provided in Figure 3. The maps indicate higher cronstedtite and lower Mg-rich serpentine abundances in the equatorial region of Bennu compared to the average prediction values. For the middle latitude region of Bennu, low cronstedtite and high Mg-rich serpentine content is predicted.

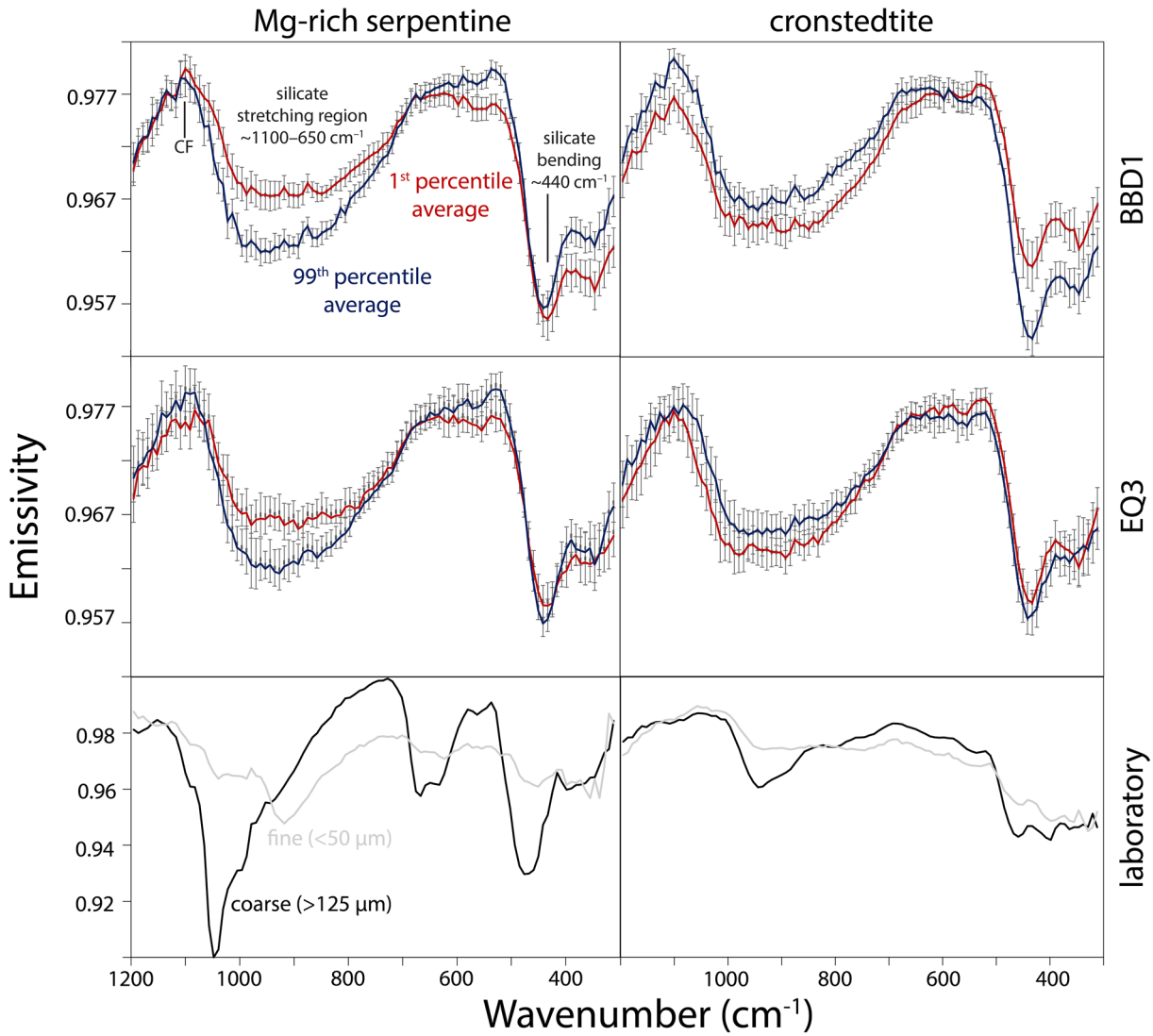

Figure 2. Average baseball diamond 1 (BBD1) (top) and equatorial station 3 (EQ3) (middle) thermal emission spectrometer (OTES) spectra of the 1st (red) and 99th (blue) percentile predictions of Mg-rich serpentine (left) and cronstedtite (right), with standard deviations. Laboratory simulated asteroid environment mid-infrared spectra (bottom) of coarse (black) and fine (gray) pure end-members using the OTES pipeline calibration (Breitenfeld et al., 2021).

Finally, we specifically examined Nightingale, the OSIRIS-REx sampling site, to understand how the phyllosilicate abundances at this location compare to Bennu overall. The selected BBD1 data set for this study does not overlap with the Nightingale sampling site. The facet of the EQ3 data set that coincides with Nightingale has prediction values of ∼54 vol% Mg-rich serpentine and ∼14 vol% cronstedtite. The Mg-rich serpentine value at Nightingale is slightly above the average prediction (52 vol%) for the EQ3 data set. The cronstedtite value at Nightingale matches the average EQ3 prediction (14 vol%). These small variations in prediction values compared to the averages fall within the model error. In addition to the EQ3 data set, we analyzed 483 OTES spectra collected within the crater of the Nightingale sampling site measured on 20 October 2020, prior to the Touch-And-Go (TAG) event (quality flags of 0–2 and fully on-body measurements). The corresponding metadata for the Nightingale spectra include MBT between ∼253 and 287 K, LTST between ∼1:48 p.m. and 3:18 p.m., and emission angles between ∼4.5 and 61.7°. From the TAG data set, the average prediction values for Mg-rich serpentine and cronstedtite are ∼53 and ∼16 vol% (Figure S3 in Supporting Information S1). The TAG Mg-rich serpentine and cronstedtite prediction values are comparable to the average values of the BBD1 and EQ3 data sets. We did not observe any compositional prediction trends with spatial position within the crater.

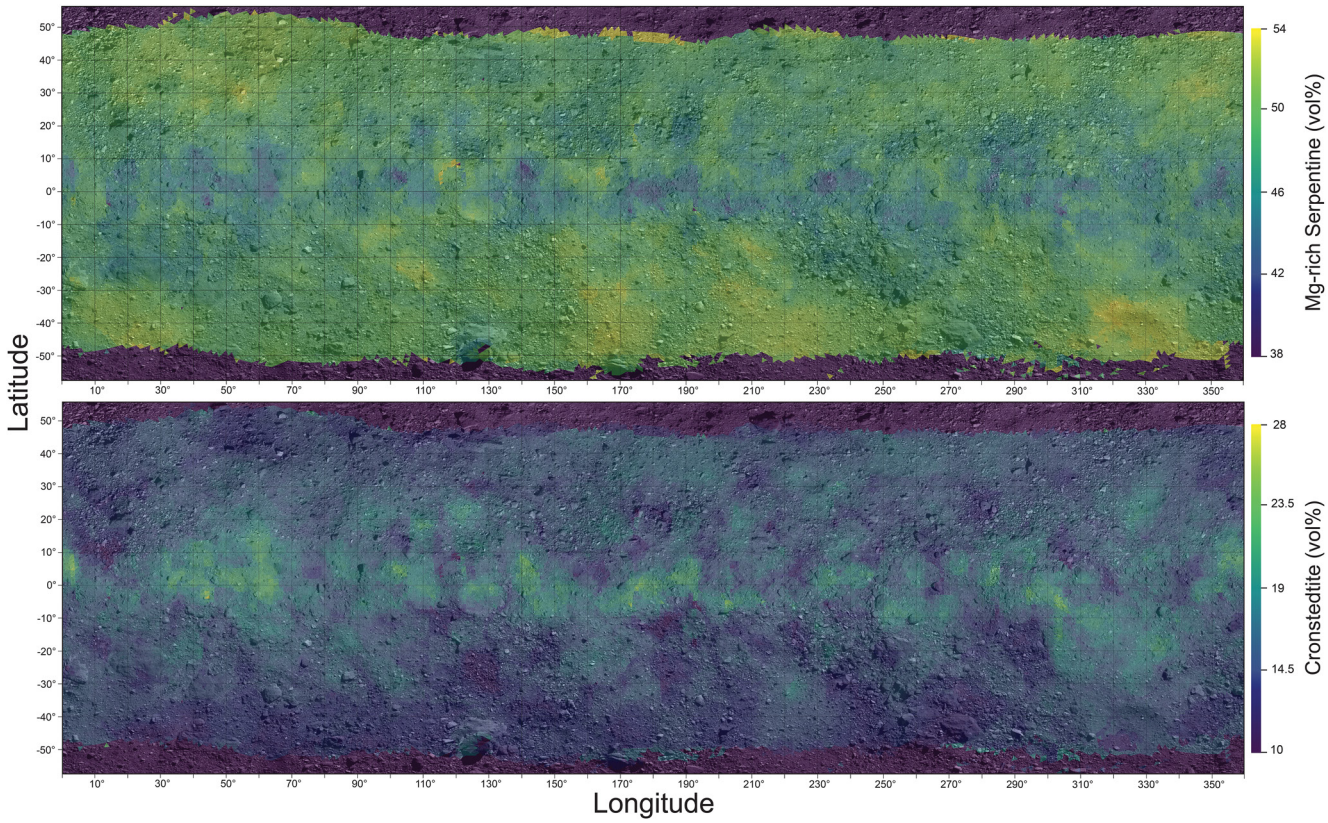

Figure 3. Bennu maps of Mg-rich serpentine (top) and cronstedtite (bottom) content from individual baseball diamond 1 (BBD1) thermal emission spectrometer (OTES) spots. Abundances derive from the phyllosilicate model that predicts Mg-rich serpentine, cronstedtite, and saponite simultaneously with a cross-validated root-mean-square error value of 15.0 vol%.

4. Discussion

4.1. Machine Learning Predictions

The average prediction values of Mg-rich serpentine, cronstedtite, and saponite are relatively consistent between the BBD1 and EQ3 datasets (Figure 1). Overall, the prediction for Mg-rich serpentine is greatest followed by cronstedtite and finally saponite. The presence and ratios of phyllosilicate minerals provide evidence for candidate materials for the asteroid Bennu.

CI chondrites typically have a mixture of serpentine and smectite whereas CM chondrites are dominated by Mg- and Fe-rich serpentines (Howard et al., 2011; King et al., 2015). Our prediction of high serpentine and low saponite content qualifies CI and CM chondrites to be considered as candidate material. More recently, Hamilton et al. (2022) has proposed considering CR1(-like) chondrites as the best match for Bennu candidate material. More specifically, Hamilton et al. (2022) showed that the mid-infrared spectrum and mineralogy from X-ray diffraction of GRO 95577 are consistent with spectra of Bennu (Hamilton et al., 2021). The mineral abundance predictions from Breitenfeld et al. (2021) have both similarities and differences with the composition of GRO 95577 (Howard et al., 2015). Finally, there are ungrouped carbonaceous chondrites that possess both serpentine and smectite minerals that may also be plausible mineralogical analogs. With the current available evidence, low petrologic type (and sub-type) CI, CM, CR, and/or ungrouped carbonaceous chondrites are all candidate materials potentially representative of Bennu (Hamilton et al., 2021; Merlin et al., 2021).

4.2. Composition Versus Particle Size

Composition and particle size affect mid-infrared spectral feature positions and depths, and therefore both must be considered when investigating spectral heterogeneity on Bennu. Hamilton et al. (2021) attribute OTES spectral

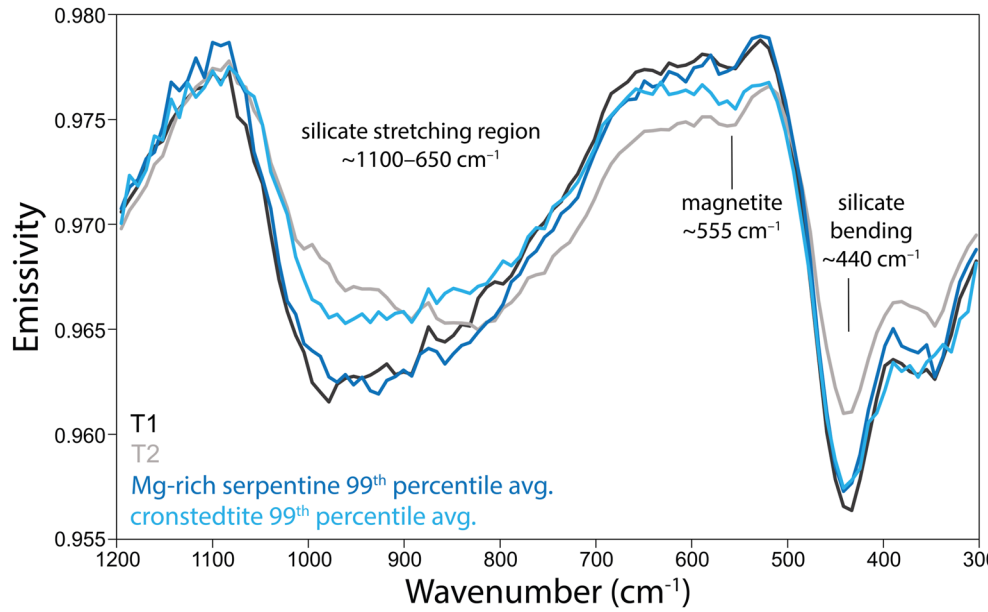

Figure 4. Comparison of T1 and T2 spectra (Hamilton et al., 2021) with the Mg-rich serpentine and cronstedtite 99th percentile averages for the equatorial station 3 (EQ3) data set.

variability primarily to particle size but also considers other properties. The particle size interpretations are based on comparisons between OTES spectra and laboratory measurements of dust deposits on solid rock substrates as well as day and nighttime measurements. In terms of composition, Hamilton et al. (2021) list five spectral characteristics to consider: CF position, silicate stretching region shape and minimum position, meteorite spectral analogs, the presence or lack of the Mg-OH plus magnetite band (~700–530 cm^{-1}), and the silicate bending feature minimum position (~440 cm^{-1}). Using these factors, Hamilton et al. (2021) compares the T1 and T2 OTES spectra to candidate analog meteorites to understand the roles of composition and particle size.

Thermal inertia can also inform the role of particle size on the OTES spectra. Rozitis et al. (2020) mapped OTES thermal inertia and indicated a band of high thermal inertia values centered at the equator of Bennu. Possible explanations include compaction and/or strength sorting due to mass movement, yet Rozitis et al. (2020) indicated that Bennu is dominated by boulders rather than regolith due to limited evidence for temperature-dependent thermal inertia. Rozitis et al. (2020) also limit the presence of fines/regolith on Bennu to <50 μm in thickness. Based on the work of Hamilton et al. (2021) and Rozitis et al. (2020), particle size and/or physical material properties likely contribute to OTES spectral shape heterogeneity.

Hamilton et al. (2021) isolated the T1 and T2 spectra from the EQ3 data set. In Figure 4, we compare the Mg-rich serpentine and cronstedtite 99th percentile averages from EQ3 to the T1 and T2 spectra. Note, spectral differences between the spectra isolated here and those produced by Hamilton et al. (2021) could arise from a discrepancy in the influencing factor (composition vs. primarily particle size). Differences between these sets of spectra include distinctions in the silicate stretching region shape, slopes between ~650 and ~530 cm^{-1}, and the 440 cm^{-1} feature depth. The slope difference between ~650 and ~530 cm^{-1} is of note given that variation in slope between the T1 and the T2 spectra is not observed. The differences between our percentile average spectra and the spectra from Hamilton et al. (2021), particularly the slope variation between ~650 and ~530 cm^{-1}, indicate that we are analyzing and mapping unique end-member spectra in comparison to the previous investigation that mapped minor variations in particle size. We did not compare our BBD1 average spectra (that have greater spectral variability) to the T1 and T2 spectra because large measurement differences exist between the two datasets.

For the Mg-rich serpentine and cronstedtite 1st and 99th percentile averages we observe several factors indicating compositional variability (Figure 2). For Mg-rich serpentine, the 99th percentile average spectrum's CF position occurs at a higher wavenumber position than that of the 1st percentile average spectrum (~8.66 cm^{-1} shift, one spectral channel). This observation is consistent with the laboratory end-member spectra for Mg-rich serpentine and cronstedtite (Figure 2, bottom), and it is expected that the CF position would shift to higher wavenumbers as

the CI/CM composition becomes more Mg-rich (Bates et al., 2020). However, note that the CF shift is small and falls within the standard deviation of the averaged spectra. Similar to the T1 and T2 spectra, the silicate stretching feature shape, position, and depth (~1,100–650 cm^{-1}) vary for the different percentile average spectra (minimum emissivity of ~0.962 for the Mg-rich serpentine 99th percentile and ~0.966 for the cronstedtite 99th percentile). The slopes between ~650 and ~530 cm^{-1} differ between the percentile average spectra (positive vs. negative for the Mg-serpentine spectra). This observation is distinct from the T1 and T2 spectra (equivalent positive slopes). Finally, the silicate bending feature minimum position (~440 cm^{-1}) differs by ~8.66 cm^{-1} for the 1st and 99th percentile averages. Aside from specific spectral features, the lack of correlation between temperature and the mineral predictions point to another factor other than particle size influencing spectral shape.

Although the phyllosilicate model that we utilize in this study predicts composition and not particle size (by design), it does fundamentally rely on spectra of materials with various particle sizes. Disentangling the roles of particle size and composition on the OTES spectra is complex due to nonlinear mixing effects of fine particulates (Salisbury & Wald, 1992; Thomson & Salisbury, 1993). It is possible that both factors contribute to OTES spectral variability. Quantifying their relative effects simultaneously is important future work to fully understand how each variable affects the OTES datasets. This could be accomplished by developing a training set specifically designed to predict both variables.

4.3. Alteration, Breakdown, and Sorting

The overall high prediction of phyllosilicate abundances on Bennu (average of ~72 vol% for both datasets) and the high proportion of Mg-bearing phyllosilicates indicates Bennu is composed of materials with evidence for high degrees of aqueous alteration (Browning et al., 1996; Howard et al., 2009). Bennu is a rubble pile asteroid that is composed of materials that experienced aqueous alteration on parent bodies rather than Bennu itself (Barnouin et al., 2019; Lauretta et al., 2019). Differences in Mg/Fe serpentine ratios across the asteroid cannot be explained solely by aqueous alteration and therefore other explanations such as breakdown and sorting must be considered.

Aqueous alteration interpretations are typically made on a meteorite rather than an asteroid size scale. Here we utilize previous detailed analyses of carbonaceous chondrites to inform the processes that created the compositional trends we predict. Typically, we would interpret serpentine-rich materials with high Mg/Fe ratios to have a higher degree of aqueous alteration than those with lower Mg/Fe ratios. Examining the components of carbonaceous chondrites, matrix materials are typically composed of primarily Fe-rich phyllosilicates given that fine particulate matrix materials are susceptible to fluid attack (Howard et al., 2011; Rubin et al., 2007; Tomeoka et al., 1989). Chondrules include Mg-rich rather than Fe-rich phyllosilicates (e.g., Nogoya and QUE 93005) as progressive alteration transitions from Fe-rich to Mg-rich phyllosilicate production (Howard et al., 2011; Rubin et al., 2007; Tomeoka et al., 1989; Velbel et al., 2012, 2015).

After aqueous alteration has occurred, factors such as mechanical breakdown/weathering and/or sorting may cause a dichotomy in the abundance of Mg- and Fe-rich phyllosilicates as a function of location on Bennu. Diurnal temperature cycles on airless bodies cause thermal breakdown of boulders, supporting a production mechanism for regolith (Molaro et al., 2020). There is also evidence on Bennu of mass movement of unconsolidated materials from the middle latitudes toward the equator (Jawin et al., 2020). Rozitis et al. (2020) suggest that the high equatorial OTES thermal inertia values may be due to strength sorting from mass movement.

Processes that have led to spatial variations in thermal inertia may have also caused mineral fractionation through physical processes enabled by initial variations in crystal size with mineral composition. In other words, sorting due to mass movement toward the equator of Bennu could contribute to spectral variability between the equatorial region and the middle latitudes, separating materials of different particle sizes while also selecting for composition (Mg/Fe ratio). More specifically, the fine particulate matrix materials could preferentially be transported through mass movement opposed to coarse particulate materials (e.g., chondrules). Replacement of olivine by serpentine pseudomorphs in chondrules (Velbel et al., 2015) results in phyllosilicate particle size variations. As previously discussed, a future investigation focused on separating the roles of composition and particle size effects would aid in testing this hypothesis. Additionally, determining if Mg-rich anhydrous silicates, associated with chondrules (e.g., forsterite), are spatially correlated with Mg-rich phyllosilicates would also test this hypothesis.

4.4. Nightingale

Nightingale, the sampling site of the OSIRIS-REx spacecraft, is of particular interest given that the scientific community will receive sample representative of this location in September 2023. Analysis of the returned sample will allow for a direct comparison between the mid-infrared laboratory measurements and the OTES remote sensing data. Our prediction of the phyllosilicate content at Nightingale from the EQ3 and TAG datasets indicates that the Mg-rich serpentine and cronstedtite abundances roughly match the compositional average surface of Bennu. We are unable to detect areas of Bennu with anomalously low or high amounts of saponite or these regions do not exist. We expect that the sample returned from Nightingale will be dominated by phyllosilicates and contain average amounts of Mg-rich serpentine, cronstedtite, and potentially saponite compared to the compositional average surface of Bennu.

5. Conclusions

Through the application of a phyllosilicate model to OTES data, we predict the phyllosilicate mineral abundances are greatest for Mg-rich serpentine followed by cronstedtite and finally saponite. For the Mg-rich serpentine and cronstedtite predictions, spectral shape is associated with the prediction values. We observe spectral heterogeneity in the EQ3 data set that is more pronounced in BBD1. We estimate higher cronstedtite and lower Mg-rich serpentine content than average in the equatorial region of Bennu and vice versa at middle latitudes. The dichotomy in Mg-rich serpentine and cronstedtite prediction values between the equatorial and middle latitude regions of Bennu may be due to breakdown, mass movement, and/or sorting effects.

Data Availability Statement

All OTES data are available in the Planetary Data System at https://arcnav.psi.edu/urn:nasa:pds:context:instrument:otes.orex (Christensen et al., 2019a). The laboratory data, model, and predictions are achieved in an external data repository at https://doi.org/10.5281/zenodo.6983992 (Breitenfeld et al., 2022).

Acknowledgments
This work was supported by the NASA OSIRIS-REx Participating Scientist program under award number 80NSSC18K0228 made to T.D. Glotch and A.D. Rogers as well as by NASA under Contract NNM10AA11C issued through the New Frontiers Program.

References

Barnouin, O. S., Daly, M. G., Palmer, E. E., Gaskell, R. W., Weirich, J. R., Johnson, C. L., et al. (2019). Shape of (101955) Bennu indicative of a rubble pile with internal stiffness. *Nature Geoscience*, *12*(4), 247–252. https://doi.org/10.1038/s41561-019-0330-x

Bates, H. C., King, A. J., Donaldson Hanna, K. L., Bowles, N. E., & Russell, S. S. (2020). Linking mineralogy and spectroscopy of highly aqueously altered CM and CI carbonaceous chondrites in preparation for primitive asteroid sample return. *Meteoritics & Planetary Sciences*, *55*(1), 77–101. https://doi.org/10.1111/maps.13411

Breitenfeld, L. B., Rogers, A. D., Glotch, T. D., Hamilton, V. E., Christensen, P. R., Lauretta, D. S., et al. (2021). Machine learning mid-infrared spectral models for predicting modal mineralogy of CI/CM chondritic asteroids and Bennu. *Journal of Geophysical Research: Planets*, *126*(12), e2021JE007035. https://doi.org/10.1029/2021je007035

Breitenfeld, L. B., Rogers, A. D., Glotch, T. D., Kaplan, H. H., Hamilton, V. E., & Christensen, P. R. (2022). Mapping phyllosilicates on the asteroid Bennu using thermal emission spectra and machine learning model applications datasets. *Zenodo*. https://doi.org/10.5281/zenodo.6983992

Browning, L. B., McSween, H. Y., Jr., & Zolensky, M. E. (1996). Correlated alteration effects in CM carbonaceous chondrites. *Geochimica et Cosmochimica Acta*, *60*(14), 2621–2633. https://doi.org/10.1016/0016-7037(96)00121-4

Christensen, P. R., Hamilton, V. E., Anwar, S., Mehall, G., & Lauretta, D. S. (2019a). Origins, spectral interpretation, Resource identification, security, regolith explorer (OSIRIS-REx): OSIRIS-REx thermal emission spectrometer bundle, NASA planetary data System.

Christensen, P. R., Hamilton, V. E., Anwar, S., Mehall, G., & Lauretta, D. S. (2019b). Origins, spectral interpretation, Resource identification, security, regolith explorer (OSIRIS-REx): OSIRIS-REx thermal emission spectrometer document collections, NASA planetary data System.

Christensen, P. R., Hamilton, V. E., Mehall, G. L., Pelham, D., O'Donnell, W., Anwar, S., et al. (2018). The OSIRIS-REx thermal emission spectrometer (OTES) instrument. *Space Science Reviews*, *214*(5), 1–39. https://doi.org/10.1007/s11214-018-0513-6

DellaGiustina, D. N., Kaplan, H. H., Simon, A. A., Bottke, W. F., Avdellidou, C., Delbo, M., et al. (2021). Exogenic basalt on asteroid (101955) Bennu. *Nature Astronomy*, *5*(1), 31–38. https://doi.org/10.1038/s41550-020-1195-z

Ferrone, S. M., Joseph, J., & Hawley, C. L. (2019). Analysis of projection effects in osiris-rex spectral mapping methods. *Mendeley*. https://doi.org/10.17632/htjvrstdx6.2

Hamilton, V. E., Christensen, P. R., Kaplan, H. H., Haberle, C. W., Rogers, A. D., Glotch, T. D., et al. (2021). Evidence for limited compositional and particle size variation on asteroid (101955) Bennu from thermal infrared spectroscopy. *Astronomy & Astrophysics*, *650*, A120. https://doi.org/10.1051/0004-6361/202039728

Hamilton, V. E., Kaplan, H. H., Connolly, H. C., Jr., Goodrich, C. A., Abreu, N. M., & Simon, A. A. (2022). GRO 95577 (CR1) as a mineralogical analogue for asteroid (101955) Bennu. *Icarus*, *383*, 115054. https://doi.org/10.1016/j.icarus.2022.115054

Hamilton, V. E., Simon, A. A., Christensen, P. R., Reuter, D. C., Clark, B. E., Barucci, M. A., et al. (2019). Evidence for widespread hydrated minerals on asteroid (101955) Bennu. *Nature Astronomy*, *3*(4), 332–340. https://doi.org/10.1038/s41550-019-0722-2

Howard, K. T., Alexander, C. O. D., Schrader, D. L., & Dyl, K. A. (2015). Classification of hydrous meteorites (CR, CM and C2 ungrouped) by phyllosilicate fraction: PSD-XRD modal mineralogy and planetesimal environments. *Geochimica et Cosmochimica Acta*, *149*, 206–222. https://doi.org/10.1016/j.gca.2014.10.025

Howard, K. T., Benedix, G. K., Bland, P. A., & Cressey, G. (2009). Modal mineralogy of CM2 chondrites by X-ray diffraction (PSD-XRD). Part 1: Total phyllosilicate abundance and the degree of aqueous alteration. *Geochimica et Cosmochimica Acta*, *73*(15), 4576–4589. https://doi.org/10.1016/j.gca.2009.04.038

Howard, K. T., Benedix, G. K., Bland, P. A., & Cressey, G. (2011). Modal mineralogy of CM chondrites by X-ray diffraction (PSD-XRD): Part 2. Degree, nature and settings of aqueous alteration. *Geochimica et Cosmochimica Acta*, *75*(10), 2735–2751. https://doi.org/10.1016/j.gca.2011.02.021

Jawin, E. R., Walsh, K. J., Barnouin, O. S., McCoy, T. J., Ballouz, R. L., DellaGiustina, D. N., et al. (2020). Global patterns of recent mass movement on asteroid (101955) Bennu. *Journal of Geophysical Research: Planets*, *125*(9), e2020JE006475. https://doi.org/10.1029/2020je006475

Kaplan, H. H., Lauretta, D. S., Simon, A. A., Hamilton, V. E., DellaGiustina, D. N., Golish, D. R., et al. (2020). Bright carbonate veins on asteroid (101955) Bennu: Implications for aqueous alteration history. *Science*, *370*(6517), eabc3557. https://doi.org/10.1126/science.abc3557

King, A. J., Schofield, P. F., Howard, K. T., & Russell, S. S. (2015). Modal mineralogy of CI and CI-like chondrites by X-ray diffraction. *Geochimica et Cosmochimica Acta*, *165*, 148–160. https://doi.org/10.1016/j.gca.2015.05.038

Kruse, F. A., Lefkoff, A. B., Boardman, J. W., Heidebrecht, K. B., Shapiro, A. T., Barloon, P. J., & Goetz, A. F. H. (1993). The spectral image processing system (SIPS)—Interactive visualization and analysis of imaging spectrometer data. *Remote Sensing of Environment*, *44*(2–3), 145–163. https://doi.org/10.1016/0034-4257(93)90013-n

Lauretta, D. S., DellaGiustina, D. N., Bennett, C. A., Golish, D. R., Becker, K. J., Balram-Knutson, S. S., et al. (2019). The unexpected surface of asteroid (101955) Bennu. *Nature*, *568*(7750), 55–60. https://doi.org/10.1038/s41586-019-1033-6

Merlin, F., Deshapriya, J. D. P., Fornasier, S., Barucci, M. A., Praet, A., Hasselmann, P. H., et al. (2021). In search of Bennu analogs: Hapke modeling of meteorite mixtures. *Astronomy & Astrophysics*, *648*, A88. https://doi.org/10.1051/0004-6361/202140343

Molaro, J. L., Walsh, K. J., Jawin, E. R., Ballouz, R. L., Bennett, C. A., DellaGiustina, D. N., et al. (2020). In situ evidence of thermally induced rock breakdown widespread on Bennu's surface. *Nature Communications*, *11*(1), 1–11. https://doi.org/10.1038/s41467-020-16528-7

Rozitis, B., Ryan, A. J., Emery, J. P., Christensen, P. R., Hamilton, V. E., Simon, A. A., et al. (2020). Asteroid (101955) Bennu's weak boulders and thermally anomalous equator. *Science Advances*, *6*(41), eabc3699. https://doi.org/10.1126/sciadv.abc3699

Rubin, A. E., Trigo-Rodríguez, J. M., Huber, H., & Wasson, J. T. (2007). Progressive aqueous alteration of CM carbonaceous chondrites. *Geochimica et Cosmochimica Acta*, *71*(9), 2361–2382. https://doi.org/10.1016/j.gca.2007.02.008

Salisbury, J. W., & Wald, A. (1992). The role of volume scattering in reducing spectral contrast of reststrahlen bands in spectra of powdered minerals. *Icarus*, *96*(1), 121–128. https://doi.org/10.1016/0019-1035(92)90009-v

Thomson, J. L., & Salisbury, J. W. (1993). The mid-infrared reflectance of mineral mixtures (7–14 μm). *Remote Sensing of Environment*, *45*(1), 1–13. https://doi.org/10.1016/0034-4257(93)90077-b

Tomeoka, K., McSween, H. Y., Jr., & Buseck, P. R. (1989). Mineralogical alteration of CM carbonaceous chondrites: A review. In *Proceedings of the NIPR symposium on antarctic meteorites* (Vol. *2*, pp. 221–234).

Velbel, M. A., Tonui, E. K., & Zolensky, M. E. (2012). Replacement of olivine by serpentine in the carbonaceous chondrite Nogoya (CM2). *Geochimica et Cosmochimica Acta*, *87*, 117–135. https://doi.org/10.1016/j.gca.2012.03.016

Velbel, M. A., Tonui, E. K., & Zolensky, M. E. (2015). Replacement of olivine by serpentine in the Queen Alexandra Range 93005 carbonaceous chondrite (CM2): Reactant–product compositional relations, and isovolumetric constraints on reaction stoichiometry and elemental mobility during aqueous alteration. *Geochimica et Cosmochimica Acta*, *148*, 402–425. https://doi.org/10.1016/j.gca.2014.10.007